

# Computed tomography-based texture assessment for the differentiation of benign, borderline, and early-stage malignant ovarian neoplasms

Journal of International Medical Research

2023, Vol. 51(1) 1–14

© The Author(s) 2023

Article reuse guidelines:

[sagepub.com/journals-permissions](https://sagepub.com/journals-permissions)

DOI: 10.1177/03000605221150139

[journals.sagepub.com/home/imr](https://journals.sagepub.com/home/imr)



Ziying He<sup>1,\*</sup>, Jia Chen<sup>2,\*</sup>, Fei Yang<sup>3</sup>,  
Xinwei Pan<sup>1</sup> and Chanzhen Liu<sup>1</sup> 

## Abstract

**Objective:** This study was performed to examine the value of computed tomography-based texture assessment for characterizing different types of ovarian neoplasms.

**Methods:** This retrospective study involved 225 patients with histopathologically confirmed ovarian tumors after surgical resection. Two different data sets of thick (5-mm) slices (during regular and portal venous phases) were analyzed. Raw data analysis, principal component analysis, linear discriminant analysis, and nonlinear discriminant analysis were performed to classify ovarian tumors. The radiologist's misclassification rate was compared with the MaZda (texture analysis software) findings. The results were validated with the neural network classifier. Receiver operating characteristic curves were analyzed to determine the performances of different parameters.

**Results:** Nonlinear discriminant analysis had a lower misclassification rate than the other analyses. Thirty texture parameters significantly differed between the two groups. In the training set, WavEnLH\_s-3 and WavEnHL\_s-3 were the optimal texture features during the regular phase, while WavEnHH\_s-4 and Kurtosis seemed to be the most discriminative features during the portal venous phase. In the validation test, benign versus malignant tumors and benign versus borderline lesions were well-distinguished.

**Conclusions:** Computed tomography-based texture features provide a useful imaging signature that may assist in differentiating benign, borderline, and early-stage ovarian cancer.

<sup>1</sup>Department of Gynecologic Oncology, Guangxi Medical University Cancer Hospital, Nanning, China

<sup>2</sup>Department of Radiology, Guangxi Medical University Cancer Hospital, Nanning, China

<sup>3</sup>Department of Clinical Medical, Guangxi Medical University, Nanning, China

\*These authors contributed equally to this work.

## Corresponding author:

Chanzhen Liu, Department of Gynecologic Oncology, Guangxi Medical University Cancer Hospital, 71 Hedi Road, Qingxiu District, Nanning 530021, China.  
Email: [liuchanzhen@gxmu.edu.cn](mailto:liuchanzhen@gxmu.edu.cn)



**Keywords**

Ovarian neoplasm, software, machine learning, tomography, texture, histopathology

Date received: 8 October 2022; accepted: 20 December 2022

**Introduction**

Ovarian neoplasms include benign, borderline, and cancerous lesions based on histopathology.<sup>1</sup> Among them, borderline ovarian tumors (BOTs) show mild nuclear atypia and cell proliferation without stromal invasion, and their biological behavior falls between that of cancerous and benign tumors.<sup>2</sup> Early-stage ovarian cancer (OC) (International Federation of Gynecology and Obstetrics [FIGO] stage I–II) has a significantly higher 5-year survival rate than other types of epithelial OC,<sup>3</sup> and it accounts for approximately 25% of all ovarian neoplasms.<sup>4,5</sup>

Ovarian tumors are usually treated surgically, and the operative plan depends on the lesion type. Benign, borderline, and malignant neoplasms often have different management plans because a conservative or fertility-sparing operation can be an option if desired.<sup>6</sup> However, the preoperative differentiation among benign, borderline, and early-stage malignant ovarian neoplasms has always been a clinical challenge because imaging cannot accurately and effectively identify these lesions. Perioperative frozen sections can guide gynecologists in selecting the optimal surgery for a given patient. A robust systematic review revealed that the concordance rates between frozen section findings and final diagnoses were 94%, 79%, and 99% for benign, borderline, and cancerous lesions, respectively.<sup>7</sup> However, intraoperative frozen section assessment has well-known limitations in diagnosing lesions such as BOTs, mucinous ovarian tumors, and large tumors.<sup>8</sup> Therefore, preoperative

and qualitative diagnosis and accurate prediction of the lesion type are crucially important for designing the best therapeutic approach.

Computed tomography (CT) uses acceptable radiation doses and is broadly applied for preoperative ovarian tumor assessment. However, the quantitative CT features that are useful for preoperative diagnosis of ovarian tumor types have rarely been examined. With the great advances that have been made in digital technologies, a new graphics assessment tool called texture analysis has been developed for analyzing medical images based on quantitative analysis of grayscale distribution parameters, inter-pixel relations, and spatial parameters.<sup>9</sup>

Texture analysis is attracting growing attention in CT-based texture analysis, which can help to evaluate and quantify tumor heterogeneity. Such a tool could noninvasively detect aggressive and treatment-resistant lesions.<sup>10</sup>

The texture features of ovarian tumors have been examined in few reports, mostly those focusing on magnetic resonance imaging and/or ultrasound. However, CT texture assessment has not been evaluated to determine its value in histologically grouping ovarian tumors.<sup>11,12</sup> We hypothesized that there are differences in the intrinsic heterogeneity among benign, borderline, and cancerous lesions and that these differences can be reflected by CT-based texture features. Therefore, we performed the present study to comparatively assess the CT-based texture parameters of benign tumors, borderline lesions, and early-stage OC and to

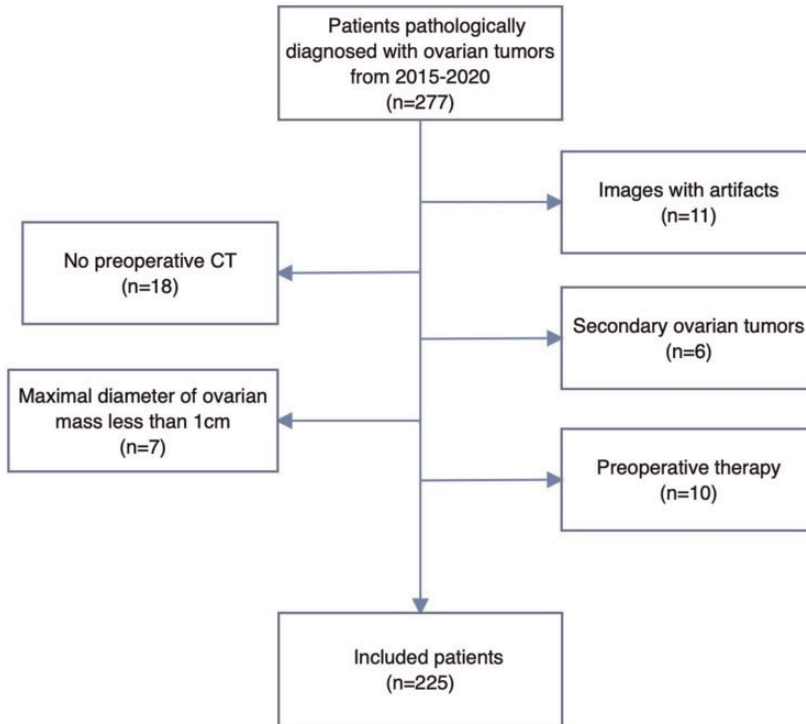


**Figure 1.** Study flowchart. CT, computed tomography.

generate a machine learning model for characterizing ovarian tumors.

## Materials and methods

*The reporting of this retrospective study conforms to the STARD guidelines.*<sup>13,14</sup>

The present study was approved by the Institutional Research Board of Guangxi Medical University Affiliated Cancer Hospital (approval no. 2021-ky-114). All patients provided written informed consent. Consecutive patients ultimately diagnosed with benign tumors, borderline lesions, or early-stage OC from December 2015 to December 2020 were analyzed. The inclusion criteria were confirmation of an ovarian tumor by surgical resection or biopsy,

availability of patient data, and complete CT data and medical history. The exclusion criteria were an ovarian mass that either had a longest diameter of <1 cm or was undetectable on CT images; pronounced CT image artifacts precluding delineation of the region of interest (ROI); secondary ovarian tumors; other cancers detected in the past 5 years; and presurgical treatments, including chemotherapy, radiotherapy, and/or local therapy. The study flowchart is presented in Figure 1. In total, 225 patients were finally included in this study. Their ages ranged from 12 to 89 years (mean,  $46.87 \pm 15.2$  years). The training set comprised 73 early malignant tumors, 35 borderline tumors, and 78 benign tumors (Table 1). Based on the above-listed eligibility criteria, 17 early malignant

**Table 1.** Demographic and clinical characteristics of patients with benign, borderline, and malignant ovarian neoplasm in the training set.

Characteristic	Benign (n = 78)	Borderline (n = 35)	Malignant (n = 73)
Age, years			
<50	49/78 (63.0)	16/35 (45.7)	38/73 (52.1)
≥50	29/78 (37.0)	19/35 (54.3)	35/73 (47.9)
Menopausal status			
Yes	27/78 (34.6)	20/35 (57.1)	30/73 (41.1)
No	51/78 (65.4)	15/35 (42.9)	43/73 (58.9)
Histology <sup>a</sup>			
Epithelial tumors	Serous (30) Mucinous (15) Seromucinous (1)	Serous (11) Mucinous (22) Seromucinous (2)	Serous (22) Mucinous (7) Seromucinous (3) Endometrioid (8) Clear cell (11)
Mesenchymal tumors	\	\	Carcinosarcoma (2)
Sex cord-stromal tumors	\	\	Granulosa cell (10)
Germ cell tumors	Mature teratoma (27)	\	Yolk sac tumor (5) Immature teratoma (1) Dysgerminoma (2) Mixed germ cell tumor (2)
FIGO stage <sup>b</sup>			
I		27	57
II		8	16

Data are presented as n (%) or n.

FIGO, International Federation of Gynecology and Obstetrics.

<sup>a</sup>Based on the 2014 World Health Organization classification of tumors of female reproductive organs.

<sup>b</sup>Based on the 2014 FIGO staging system.

tumors, 5 borderline tumors, and 17 benign tumors diagnosed in 2020 were enrolled in the validation set.

High-resolution CT was carried out with 64-row detector (Discovery CT750 HD; GE Healthcare, Chicago, IL, USA) and 128-channel CT (Discovery CT750; GE Healthcare) scanners using the following parameters: field of view, 25 cm; matrix, 512 × 512; tube voltage, 120 kVp; tube current, 200 to 400 mA; rotation, 0.5 s, pitch, 0.984:1; and interval, 1.3 mm. The contrast agent (iodine, 350 mg/mL) was administered at a dose of 2 mL/kg (but not exceeding 100 mL) and rate of 2 mL/s. The portal venous phase (PVP) of contrast-enhanced CT images was obtained. The slice thickness was 0.625 mm, and image

reconstruction to 5-mm thickness was carried out. All CT data were anonymized prior to upload to the texture analysis software (V4.6; Instytut Elektroniki, <http://www.eletel.p.lodz.pl/mazda/>).

The CT images were reviewed by two radiologists with 3 and 30 years of experience in abdominal CT data analysis, respectively. The radiologists were blinded to the patients' data and performed the classifications in an independent manner.

A picture archiving and communication system was utilized for image storage. The slice with the greatest tumor diameter underwent exportation as a .bmp file. ROIs were consensually delineated by two evaluators: the images that most overtly displayed the tumor boundary were utilized

for drawing the ROI, which was copied and pasted onto another image with necessary adjustments; the two-dimensional ROI was then manually placed within the lesion boundary (Figure 2). In challenging cases (obscure lesions on CT scans), magnetic resonance imaging was applied when available.

A texture analysis of axial regular and enhanced CT scans in the PVP was carried out. CT-based texture analysis was performed with MaZda v4.6, which is a commercially available software.<sup>15</sup> The image gray-level intensity was normalized as reported previously. This package included image processing, extraction, and selection of texture features. To minimize the influence of contrast and brightness variation, image gray-level intensity normalization was performed using a method that normalizes image intensities within a range ( $\mu - 3\delta$ ,  $\mu + 3\delta$ ;  $\mu$ , mean gray level value;  $\delta$ , standard deviation; both  $\mu$  and  $\delta$  are computed separately for every ROI) in MaZda.<sup>16</sup>

MaZda helped to compute roughly 300 texture parameters based on the image histogram, co-occurrence matrix (COM), run-length matrix, image gradient, autoregressive model, and Haar wavelet (WAV). Fisher's coefficient (F), classification error probability combined with average correlation coefficients (P), and mutual information (M) were jointly applied (FPM) to identify the 30 texture parameters with the greatest potential in distinguishing lesions.

The 30 parameters were obtained from the target images and further processed and classified with module B11 of MaZda. The image reflecting the greatest lesion area was selected, with the lesion boundary consensually delineated by the above-mentioned radiologists.

The feature standardization option of module B11 was utilized (mean value by standard deviation). Raw data analysis

(RDA), principal component analysis (PCA), linear discriminant analysis (LDA), and nonlinear discriminant analysis (NDA) were performed for all image subsets to group the texture features. The default neural network features of module B11 were applied. Nearest-neighbor classification was carried out to assess raw data, with the most expressive and discriminating parameters determined by PCA and LDA, respectively. NDA was performed to classify the features by an artificial neural network. These classification procedures were conducted by using RDA, PCA, LDA, and NDA on module B11, and misclassification rates were calculated.

Additionally, a senior radiologist blinded to the software analysis and histopathological diagnoses grouped the cases into benign, BOT, and early malignant cases in an independent fashion, and the misclassification rate was determined. After comparing the RDA, PCA, LDA, and NDA results for the misclassification rate, the method with the highest accuracy was compared with the radiologist's findings.

The validation set was examined based on the same 30 texture parameters, and misclassification rates were determined.

Parametric tests were performed to assess continuous variables due to the central limit theorem of conformity.<sup>17</sup> Numerical data with normal and skewed distributions are presented as mean  $\pm$  standard deviation and median with interquartile range, respectively, and were compared using the independent-samples t-test and the Mann-Whitney U-test, respectively. Categorical data were compared using Pearson's chi-square test or Fisher's exact test. Qualitative data were analyzed with the chi-square test. The independent-samples t-test or independent Mann-Whitney U test was utilized to determine whether the 30 texture parameters obtained from each phase had significant differences among benign, BOT, and early malignant

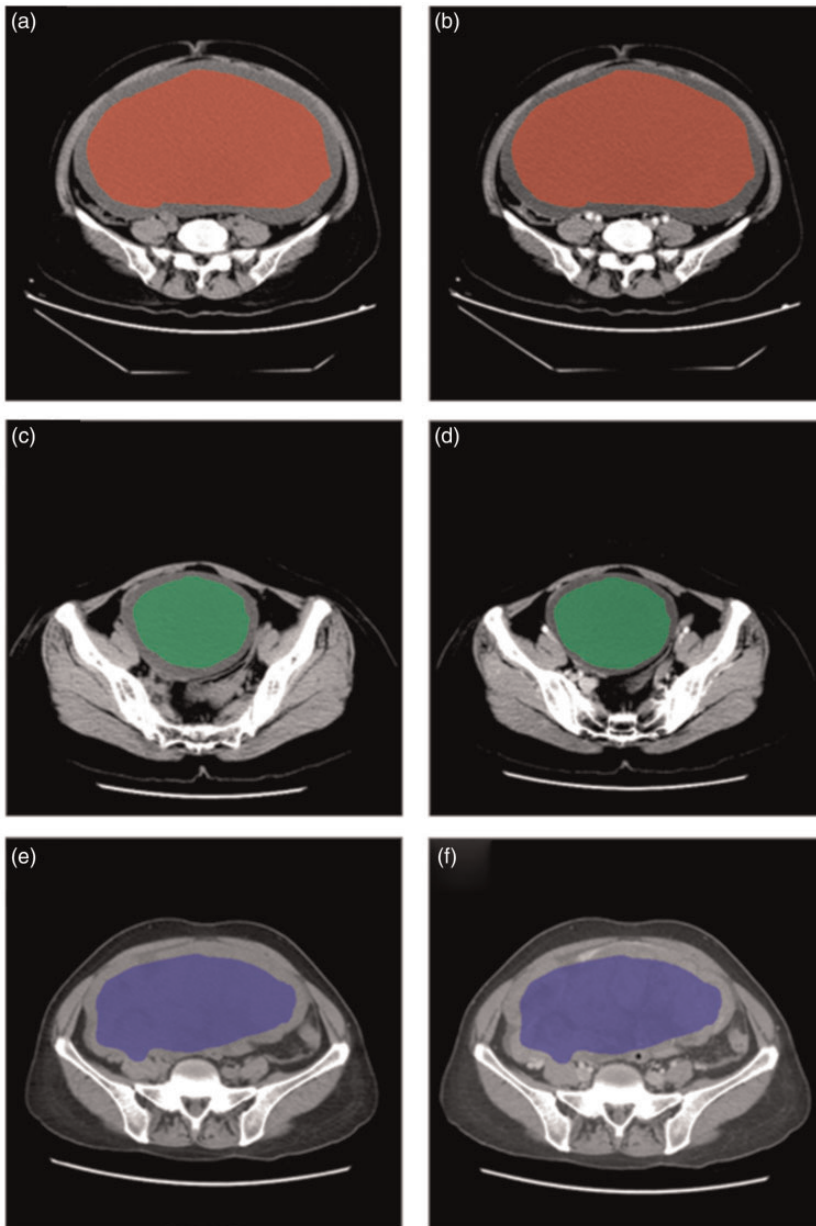


**Figure 2.** (a, b) Images of a 31-year-old woman with an ovarian serous benign tumor. Regular and portal venous phase (PVP) images show the main lesion in the red region of interest (ROI). (c, d) Images of a 45-year-old woman with an ovarian serous borderline lesion. Regular and PVP images show the main lesion in the green ROI and (e, f) Images of a 67-year-old woman with an ovarian seromucinous borderline lesion. Regular and PVP images show the main mass in the blue ROI.



cases. Receiver operator characteristic curve analysis was performed to determine the areas under the receiver operating characteristic curves (AUCs). A p-value of  $<0.05$  indicated statistical significance. SPSS 26.0 (IBM Corp., Armonk, NY, USA) was utilized for data analysis.

## Results

### *Clinicopathologic findings in the training set*

In total, 186 individuals were included in the training set (Table 1). The median ages of patients with benign lesions, BOTs, and early malignant lesions were 43.5 (range, 16–76), 48.7 (range, 15–78), and 48.9 (range, 12–80) years, respectively ( $p < 0.001$ ). Table 1 summarizes all clinicopathologic features. Most lesions were of epithelial origin. The early malignant cancers included 57 stage I and 16 stage II cases, whereas the borderline lesions included 27 stage I and 8 stage II cases. Table 2

summarizes the morphological parameters of all ovarian lesions. The configuration, maximum diameter of the lesions, and number of loculi were significantly different between any two types ( $p < 0.05$ ).

### *Training set*

Table 3 shows the grouping data for benign versus borderline, borderline versus early malignant, and benign versus early malignant lesions in various imaging phases based on MaZda. In the comparison of RDA, PCA, LDA, and NDA, NDA showed the lowest misclassification rate. The lowest misclassification rate was 5/151 (3.31%), which occurred with NDA of the regular phase in differentiating between benign and early malignant cases. However, the misclassification rates were similar in NDA between the regular phase and PVP for distinguishing between borderline and early malignant cases and between benign and early malignant cases. Of these methods, NDA had a lower misclassification rate than RDA, PCA, and LDA.

**Table 2.** Morphological CT parameters of ovarian lesions in the training set.

CT features	Benign (n = 78)	Borderline (n = 35)	Malignant (n = 73)	p-value*
Morphology				0.114
Lobulated	47/78	20/35	32/73	
Round/oval	31/78	15/35	41/73	
Configuration				<0.001
Purely cystic	20/78	5/35	7/73	
Predominantly cystic	34/78	7/35	9/73	
Mixed cystic/solid	22/78	20/35	45/73	
Predominantly solid or solid	2/78	3/35	12/73	
Maximum diameter of lesions, cm				<0.001
<7	42/78	5/35	12/73	
≥7	36/78	30/35	61/73	
Number of loculi				0.001
Unilocular	25/78	5/35	6/73	
Multilocular	40/78	26/35	47/73	
Honeycomb loculi	13/78	4/35	20/73	

CT, computed tomography.

Data are presented as n.

\*Different values among the three groups.

**Table 3.** Misclassification rates in the training set for ovarian tumor grouping using FPM.

	Regular			Portal venous phase		
	Benign vs. BOT	Borderline vs. malignant	Benign vs. malignant	Benign vs. BOT	Borderline vs. malignant	Benign vs. malignant
RDA	29/113 (25.66)	44/108 (40.74)	33/151 (21.85)	35/113 (30.97)	42/108 (38.89)	43/151 (28.48)
PCA	27/113 (23.89)	44/108 (40.74)	34/151 (22.51)	36/113 (31.86)	41/108 (37.96)	45/151 (29.80)
LDA	20/113 (17.75)	25/108 (23.15)	20/151 (13.25)	21/113 (18.58)	36/108 (33.33)	23/151 (15.32)
NDA	8/113 (7.08)	18/108 (16.67)	5/151 (3.31)	18/113 (15.93)	17/108 (15.74)	6/151 (3.97)

Data are presented as number of misclassifications/total cases (%). In total, 186 cases were included in the training set. RDA, PCA, LDA, and NDA were utilized for assessment in the regular and portal venous phases. Classifications were performed according to FPM.

FPM, combination of Fisher's coefficient (F), classification error probability and average correlation coefficients (P), and mutual information (M); BOT, borderline ovarian tumor; LDA, linear discriminant analysis; NDA, nonlinear discriminant analysis; PCA, principal component analysis; RDA, raw data analysis.

**Table 4.** Texture parameters with AUCs>0.7 and P values based on the independent Mann-Whitney U test in the training set.

	Regular			Portal venous phase		
	Feature	p-value	AUC	Feature	p-value	AUC
Benign vs. borderline	WavEnHH_s-4 (WAV)	<0.001	0.841	WavEnHH_s-4 (WAV)	<0.001	0.791
	WavEnLH_s-3 (WAV)	<0.001	0.846	WavEnHH_s-5 (WAV)	<0.001	0.754
				WavEnHL_s-3 (WAV)	<0.001	0.780
				WavEnHL_s-4 (WAV)	<0.001	0.788
Borderline vs. malignant	None			Kurtosis (COM)	0.001	0.700
Benign vs. malignant	WavEnHL_s-2 (WAV)	<0.001	0.724	None		
	WavEnHL_s-3 (WAV)	<0.001	0.857			

AUC, area under the receiver operating characteristic curve; COM, co-occurrence matrix; WAV, wavelets transform.

Additionally, in both the regular phase and PVP, the four methods significantly differed in distinguishing among benign, borderline, and early malignant cases ( $p < 0.01$ ). The lowest misclassification rate obtained by the radiologist was 29.03% (54/186) in differential diagnosis between benign and early malignant cases; this rate was markedly higher than that of NDA for all sequences ( $p < 0.05$ ).

AUCs were determined for all texture parameters showing significant differences; those with an AUC of  $>0.7$  are shown in Table 4. WAV-based and COM-based parameters had good classification values. There were four WAV-based and one

COM-based feature in the PVP (WavEnHH\_s-4, WavEnHH\_s-5, WavEnHL\_s-3, WavEnHL\_s-4, and Kurtosis) and four WAV-based features in the regular phase (WavEnHH\_s-4, WavEnLH\_s-3, WavEnHL\_s-2, and WavEnHL\_s-3). The most discriminating features were WavEnLH\_s-3 (WAV) and WavEnHL\_s-3 (WAV) in the regular phase for distinguishing between benign and borderline cases (WavEnLH\_s-3: AUC, 0.846) (Figure 3(a)) and between benign and early malignant cases (WavEnHL\_s-3: AUC, 0.857) (Figure 3(b)). WavEnHH\_s-4 and Kurtosis were the most discriminating features in the PVP for distinguishing between benign and borderline



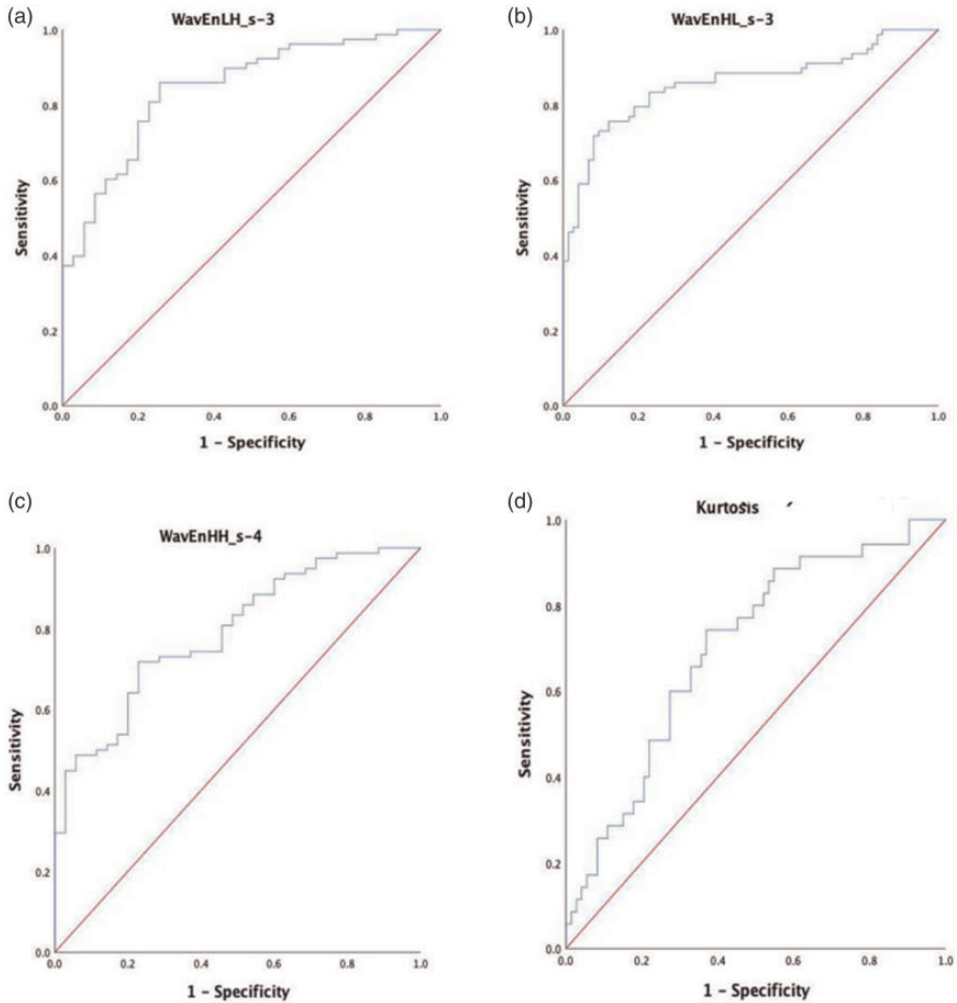


**Figure 3.** (a) Receiver operator characteristic (ROC) curve for WavEnLH\_s-3 on regular images in the training set. (b) ROC curve for WavEnHL\_s-3 on regular images in the training set. (c) ROC for WavEnHH\_s-4 on portal venous phase (PVP) images in the training set and (d) ROC for Kurtosis on PVP images in the training set.

cases (WavEnHH\_s-4: AUC, 0.791) (Figure 3(c)) and between borderline and early malignant cases (Kurtosis: AUC, 0.700) (Figure 3(d)).

### Validation set

Table 5 summarizes the grouping results in the validation set for different CT scan

phases. These validation data accurately distinguished between benign and borderline cases in the regular phase [misclassification rate: 0.0% (0/22)], between borderline and early malignant cases [misclassification rate: 4.5% (1/22)], and between benign and early malignant cases [misclassification rate: 0.0% (0/34)]. However, regular phase and PVP data were not markedly different.

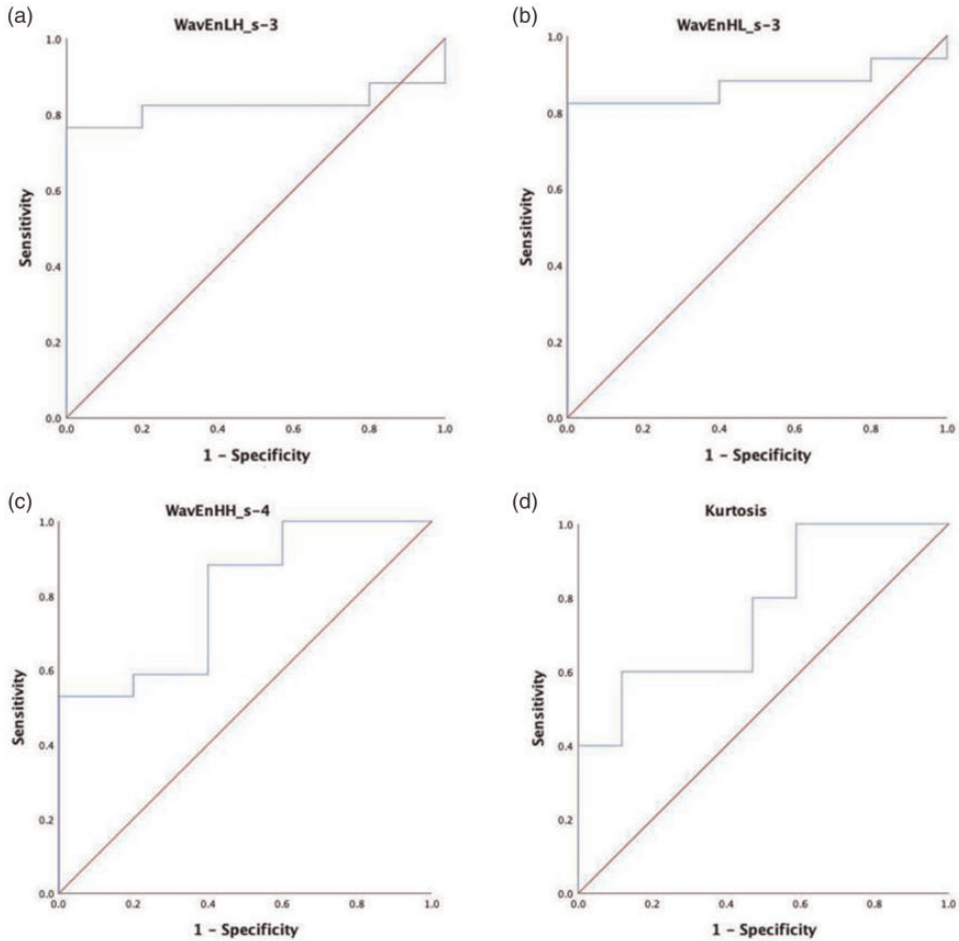


**Figure 4.** (a) Receiver operator characteristic (ROC) curve for WavEnLH\_s-3 on regular images in the validation set. (b) ROC for WavEnHL\_s-3 on regular images in the validation set. (c) ROC for WavEnHH\_s-4 on portal venous phase (PVP) images in the validation set and (d) ROC for Kurtosis on PVP images in the validation set.

Figure 4 shows the results of WavEnLH\_s-3, WavEnHL\_s-3, WavEnHH\_s-4, and Kurtosis in differentiating benign, borderline, and early malignant cases in the validation set. The performances of WavEnLH\_s-3, WavEnHL\_s-3, and WavEnHH\_s-4 remained good in the external validation. In the regular phase, WavEnLH\_s-3 distinguished between benign and borderline cases (WavEnLH\_s-3: AUC, 0.824) (Figure 4(a)) while

WavEnHL\_s-3 distinguished between benign and early malignant cases (WavEnHL\_s-3: AUC, 0.720) (Figure 4(b)) with the highest performances. In the PVP, WavEnHH\_s-4 best distinguished between benign and borderline cases (WavEnHH\_s-4: AUC, 0.800) (Figure 4(c)). However, Kurtosis extracted from the PVP did not differ significantly between borderline and early malignant cases (Kurtosis: AUC, 0.765) (Figure 4(d)).

**Table 5.** Misclassification rates of the validation set for differentiating ovarian neoplasms.

	Regular			Portal venous phase		
	Benign vs. borderline	Borderline vs. malignant	Benign vs. malignant	Benign vs. borderline	Borderline vs. malignant	Benign vs. malignant
Misclassification rates	0/22 (0.0)	1/22 (4.5)	0/34 (0.0)	2/22 (10.53)	1/22 (4.5)	0/34 (0.0)

Data are presented as number of misclassifications/total cases (%). In total, 39 cases were included in the validation set. The neural network classifier was utilized for assessment with the module B11.

## Discussion

### Summary of main results

In the present study, by analyzing the texture features of CT images of ovarian tumors in the regular phase and PVP, we found that use of the radiomics features based on CT texture assessment could help to distinguish among benign, borderline, and early malignant cases. Different statistical techniques (i.e., RDA, PCA, LDA, and NDA) were used for differentiating benign, borderline, and early malignant cases based on regular and PVP images in the training set. As shown above, NDA had a markedly lower misclassification rate than the other methods in the regular phase and PVP ( $p < 0.01$ ) for differentiating benign, borderline, and cancerous ovarian neoplasms. The goal of NDA is to identify a nonlinear transformation of various feature vectors for projecting the input patterns on a space (potentially with lower dimensionality, as for PCA and LDA) in which linear separation occurs. The texture features of regular images showed the lowest misdiagnosis rates of 7.08% and 3.31% for benign versus borderline and benign versus malignant, respectively, and therefore had the best performance in distinguishing among them. However, the texture features obtained from PVP images better distinguished between borderline and cancerous neoplasms (misdiagnosis rate: 15.74%).

In this study, four texture feature classifications (WavEnLH\_s-3, WavEnHL\_s-3, WavEnHH\_s-4, and Kurtosis) were vital factors for characterizing benign, borderline, and early malignant cases. As shown above, compared with borderline cases, Kurtosis in the PVP was markedly elevated for early-stage OC, suggesting that the PVP value's maximum frequency is remarkably elevated; in other words, microvascular perfusion areas are starkly greater in early-stage OC than in borderline cases. The above results corroborate previous observations in other cancers.<sup>18</sup> Unfortunately, Kurtosis did not exhibit a statistically significant difference in differentiating borderline and early-stage OC in the validation set. The reason may be the relatively small number of cases in the validation set. As shown above, WavEnLH\_s-3 values were markedly higher in borderline than in benign cases, WavEnHL\_s-3 was higher in early malignant than in benign cases, and WavEnHH\_s-4 was higher in borderline than in benign cases. Wavelet transform could identify fine structural details not detectable by the naked eye (e.g., by amplifying subtle intensity variations between areas while representing homogeneity intensity within an area). Therefore, the histopathological properties of ovarian neoplasms might be associated with frequency signals in CT, which deserves further investigation.

### *Results in the context of published literature*

CT is widely utilized for evaluating the severity of disease and monitoring the therapeutic response in patients with ovarian tumors. Radiologists routinely perform subjective assessments of CT scans according to their experience for diagnosing or evaluating ovarian tumors.<sup>19</sup> Tumor heterogeneity is an essential property of cancer and is driven by highly altered tissue architecture due to infiltrated cells, necrosis, anomalous angiogenesis, and myxoid alterations.<sup>20</sup> Tumor heterogeneity evaluated by CT-based texture assessment is a novel tool for postprocessing CT data and generating novel quantitation features that associate qualitative and/or quantitative imaging data with diagnosis, staging, prognostication, and treatment-response assessment in various cancers.<sup>21–23</sup>

In previous studies, CT texture assessment was considered to provide promising imaging biomarkers of OC, helping to predict histopathological features, therapeutic response, and prognosis.<sup>24–26</sup> Among statistical techniques, NDA has been shown to be effective for assessing texture features in various diseases,<sup>27,28</sup> consistent with the results of the present study. Among the many features, Wavelet transform, a routine tool for texture analysis, converts signals from the time domain to the frequency domain, revealing the tissue characteristic properties of enhancement kinetics. It is a potent tool for distinguishing non-malignant from cancerous lesions.<sup>29</sup> Kurtosis reflects the peak of the gray-scale histogram based on the tissue pixel distribution and indicates the PVP size at maximum frequency.<sup>30</sup> To date, however, CT-based texture analysis has not been applied to compare benign, BOT, and early malignant ovarian neoplasms.

### *Strengths and weaknesses*

This study focused on the preoperative differentiation and evaluation of ovarian neoplasms through texture analysis of CT radiomics; i.e., we investigated the diagnostic performance of texture for characterizing ovarian tumors. The results showed for the first time that CT texture features could distinguish among benign, borderline, and early-stage malignant ovarian neoplasms. This will allow doctors to more effectively assess the properties of ovarian neoplasms by CT examination.

This study had several limitations. First, it was a single-center trial involving a limited number of patients. Additionally, standardized and consistent CT parameters were applied, decreasing the generalizability of the study findings. **Although all AUC values in our model were ideal, the introduction of an externally validated data set would improve the universality of the results.** Second, texture features were only examined on two-dimensional images, focusing on sections with maximum tumor diameters in all cases. Despite its wide application, such a strategy might not properly account for the whole tumor as would a three-dimensional analysis. Third, we did not assess interobserver variability. The significant associations of texture features with ovarian lesions in the validation set were based on few patients, and these data should be validated in large multicenter trials. Additional software enabling three-dimensional texture assessment would also complement these findings.

### *Implications for practice and future research*

In conclusion, CT texture features could distinguish among benign, borderline, and early-stage malignant ovarian neoplasms,

and NDA showed the lowest misclassification rate for both regular and PVP images. Regular images might be more informative for distinguishing between benign and borderline cases or between benign and early malignant cases, as demonstrated in the training and validation sets. Kurtosis is an optimal texture feature on PVP images for distinguishing between borderline and early-stage OC. WAV-based parameters were shown to be most discriminative.

### Author contributions

CL and PW were responsible for the conception and design of the experiments. HY, JC, and FY contributed to the acquisition, analysis, and interpretation of the data. HY and JC wrote the manuscript. All authors have read and approved the final manuscript.

### Data availability statement

The data used to support the findings of this study are available from the corresponding author upon request.

### Declaration of conflicting interests

The authors declare that there is no conflict of interest.

### Funding

The authors disclose receipt of the following financial support for the research, authorship, and/or publication of this article: This work was supported in part by grants from the Natural Science Foundation of Guangxi Zhuang Autonomous Region (nos. 2018GXNSFBA138048 and 2019GXNSFAA245073).

### ORCID iD

Chanzhen Liu  <https://orcid.org/0000-0002-3606-7202>

### References

1. Lalwani N, Prasad SR, Vikram R, et al. Histologic, molecular, and cytogenetic

features of ovarian cancers: implications for diagnosis and treatment. *Radiographics* 2011; 31: 625–646.

2. Naqvi J, Nagaraju E and Ahmad S. MRI appearances of pure epithelial papillary serous borderline ovarian tumours. *Clin Radiol* 2015; 70: 424–432.
3. Hennessy BT, Coleman RL and Markman M. Ovarian cancer. *Lancet* 2009; 374: 1371–1382.
4. Sung H, Ferlay J, Siegel RL, et al. Global cancer statistics 2020: GLOBOCAN estimates of incidence and mortality worldwide for 36 cancers in 185 countries. *CA Cancer J Clin* 2021; 71: 209–249.
5. Torre LA, Trabert B, DeSantis CE, et al. Ovarian Cancer Statistics, 2018. *Ca-Cancer J Clin* 2018; 68: 284–296.
6. Armstrong DK, Alvarez RD, Bakkum-Gamez JN, et al. Ovarian Cancer, Version 2.2020, NCCN Clinical Practice Guidelines in Oncology. *J Natl Compr Canc Netw* 2021; 19: 191–226.
7. Ratnavelu ND, Brown AP, Mallett S, et al. Intraoperative frozen section analysis for the diagnosis of early stage ovarian cancer in suspicious pelvic masses. *Cochrane Database Syst Rev* 2016; 3: CD010360.
8. Park JY, Lee SH, Kim KR, et al. Accuracy of frozen section diagnosis and factors associated with final pathological diagnosis upgrade of mucinous ovarian tumors. *J Gynecol Oncol* 2019; 30: e95.
9. Tu W, Sun G, Fan L, et al. Radiomics signature: a potential and incremental predictor for EGFR mutation status in NSCLC patients, comparison with CT morphology. *Lung Cancer* 2019; 132: 28–35.
10. Tang L, Wang XJ, Baba H, et al. Gastric cancer and image-derived quantitative parameters: part 2—a critical review of DCE-MRI and (18)F-FDG PET/CT findings. *Eur Radiol* 2020; 30: 247–260.
11. Nougaret S, Tardieu M, Vargas HA, et al. Ovarian cancer: an update on imaging in the era of radiomics. *Diagn Interv Imaging* 2019; 100: 647–655.
12. Ye RP, Weng SP, Li YM, et al. Texture analysis of three-dimensional MRI images

- may differentiate borderline and malignant epithelial ovarian tumors. *Korean J Radiol* 2021; 22: 106–117.
13. Bossuyt PM, Reitsma JB, Bruns DE, et al. STARD 2015: an updated list of essential items for reporting diagnostic accuracy studies. *BMJ (Clinical research ed)* 2015; 351: h5527.
  14. Von Elm E, Altman DG, Egger M, et al. The Strengthening the Reporting of Observational Studies in Epidemiology (STROBE) statement: guidelines for reporting observational studies. *Ann Intern Med* 2007; 147: 573–577.
  15. Szczypiński PM, Strzelecki M, Materka A, et al. MaZda—a software package for image texture analysis. *Comput Methods Programs Biomed* 2009; 94: 66–76.
  16. Shafiq-Ul-Hassan M, Zhang GG, Latifi K, et al. Intrinsic dependencies of CT radiomic features on voxel size and number of gray levels. *Med Phys* 2017; 44: 1050–1062.
  17. Liu S, Shi H, Ji C, et al. Preoperative CT texture analysis of gastric cancer: correlations with postoperative TNM staging. *Clin Radiol* 2018; 73: 756 e751–756 e759.
  18. Jin YN, Zhang Y, Cheng JL, et al. The role of histogram analysis in diffusion-weighted imaging in the differential diagnosis of benign and malignant breast lesions. *BMC Med Inform Decis Mak* 2020; 20: 239.
  19. Nougaret S, McCague C, Tibermacine H, et al. Radiomics and radiogenomics in ovarian cancer: a literature review. *Abdom Radiol (NY)* 2021; 46: 2308–2322.
  20. Rizzo S, Botta F, Raimondi S, et al. Radiomics: the facts and the challenges of image analysis. *Eur Radiol Exp* 2018; 2: 36.
  21. Botta F, Raimondi S, Rinaldi L, et al. Association of a CT-based clinical and radiomics score of non-small cell lung cancer (NSCLC) with lymph node status and overall survival. *Cancers (Basel)* 2020; 12: 1432.
  22. Li M, Sun K, Dai W, et al. Preoperative prediction of peritoneal metastasis in colorectal cancer using a clinical-radiomics model. *Eur J Radiol* 2020; 132: 109326.
  23. Hu T, Wang S, Huang L, et al. A clinical-radiomics nomogram for the preoperative prediction of lung metastasis in colorectal cancer patients with indeterminate pulmonary nodules. *Eur Radiol* 2019; 29: 439–449.
  24. Martin-Gonzalez P, Crispin-Ortuzar M, Rundo L, et al. Integrative radiogenomics for virtual biopsy and treatment monitoring in ovarian cancer. *Insights Imaging* 2020; 11: 94.
  25. Rizzo S, De Piano F, Buscarino V, et al. Preoperative evaluation of epithelial ovarian cancer patients: role of whole body diffusion weighted imaging MR and CT scans in the selection of patients suitable for primary debulking surgery. A single-centre study. *Eur J Radiol* 2020; 123: 108786.
  26. Li M, Tan J, Zhang Y, et al. Assessing CT imaging features combined with CEA and CA125 levels to identify endometriosis-associated ovarian cancer. *Abdom Radiol (NY)* 2021; 46: 2367–2375.
  27. Li X, Zhu H, Qian X, et al. MRI texture analysis for differentiating nonfunctional pancreatic neuroendocrine neoplasms from solid pseudopapillary neoplasms of the pancreas. *Acad Radiol* 2020; 27: 815–823.
  28. Liu J, Pei Y, Zhang Y, et al. Predicting the prognosis of hepatocellular carcinoma with the treatment of transcatheter arterial chemoembolization combined with microwave ablation using pretreatment MR imaging texture features. *Abdom Radiol (NY)* 2021; 46: 3748–3757.
  29. Liu YB, Zheng JB, Zhao JZ, et al. Magnetic resonance image biomarkers improve differentiation of benign and malignant parotid tumors through diagnostic model analysis. *Oral Radiol* 2021; 37: 658–668.
  30. Li L, Zhao JS, Gao ZF, et al. [Application of apparent diffusion coefficient in children aged 2–12 years with intellectual disability/global developmental delay who have normal conventional brain MRI findings]. *Zhongguo Dang Dai Er Ke Za Zhi* 2019; 21: 541–546.